Progress In Electromagnetics Research M, Vol. 63, 93–105, 2018

Improving the Efficiency of Electrical High-rpm Generators with Permanent Magnets and Tooth Winding

Flur R. Ismagilov, Vyacheslav E. Vavilov, and Ruslan D. Karimov*

Abstract—This paper solves the problem of minimizing losses in the stator magnetic core of high-speed electric machines with the use of amorphous iron. A fundamentally new technology for manufacturing of a stator magnetic core from segments of amorphous steel is developed by the authors. The feature of the new stator design is the possibility to use technological ducts located inside the stator as cooling ducts. This aspect significantly improves the heat dissipation from the active zone of the stator and, accordingly, minimizing temperature. The efficiency of this solution was studied using two power generators of 100 kW and 200 kW and rotational speeds of 60,000 rpm and 45,000 rpm respectively in the software complex Ansys Maxwell. Harmonic compositions of currents and voltages, flux density distributions in active elements of the generator in various operating modes were studied: under load, in a three-phase short-circuit and at idle. Also, the obtained data were compared with analogous models of an electrogenerator made of electrical steel. The results of the study showed the operability and effectiveness of the proposed technology. Based on the results of the research, a prototype of the stator magnetic core made from amorphous iron was created. Losses in the generator were experimentally measured. Also the results of experimental studies of aerodynamic losses are presented.

1. INTRODUCTION

Improving the energy efficiency of the stand-alone facilities (SAF) (transport, aerospace aircrafts, ships, distributed power generation plants) is one of the main areas of their development. An important component of SAF, affecting both functioning of SAF and the energy efficiency is its power generator or the motor-generator [1].

Recent trends show that high-rpm synchronous electrical machines with permanent magnets (HSEMPM) with a power of 50 to 300 kW and a rotor speed of 45,000 to 96,000 rpm are the most effective for use in SAF as power generators. The efficiency of their use is due to the fact that they provide direct connection with a SAF power plant, such as the gas turbine. This eliminates the unreliable reducer with big weight, overall dimensions and a significant cost. High HSEMPM rotor speed allows obtaining the maximum electric power at the minimum weight of the electrical machine, and the weight is one of the main criteria determining the SAF effectiveness. HSEMPM also does not require additional power for excitation. Thanks to all these benefits, HSEMPM is widely used in aircrafts such as F-35 [2], spacecrafts and satellites [3–5], in hybrid vehicles [6–8], ships, machine-tool industry, turbochargers, and medicine. HSEMPM are also used in virtually all distributed power generation plants (Capstone, Elliot, Turbec) [9–12].

It is clear that higher energy efficiency of HSEMPM leads to higher energy efficiency of all SAF as a whole. Therefore, research on the reduction of losses in HSEMPM has been widely discussed [13–22]. Papers of Borisavljevica et al., Munteanu et al., and others provide general approaches to the HSEMPM loss analysis, losses in the rotor permanent magnets are studied, as well as aerodynamic

Received 22 August 2017, Accepted 3 November 2017, Scheduled 7 December 2017
* Corresponding author: Ruslan D. Karimov (ruslan-k88@yandex.ru).
The authors are with the Department of Electromechanics, Ufa State Aviation Technical University, Russian Federation.

losses, and losses in HSEMPM winding [13–18]. Papers [18–20] provide studies of losses in HSEMPM with tooth winding. The advantage of this type of electric machines, in addition to all the above, is the minimum dimensions of the frontal parts, which makes them virtually the only effective solution for the transport and aerospace industries [21]. However, a significant disadvantage is an increase in the losses for eddy currents in permanent magnets due to spatial harmonics.

Paper [22] is of interest, wherein the numerical evaluation of the losses in HSEMPM with a power of 120 kW and a rotor speed of 70,000 rpm with distributed winding is given. The results of [22] are verified experimentally. It can be seen from [22] that for HSEMPM with a power of 120 kW and a rotor speed of 70,000 rpm, the losses in the stator winding account for 30% of the total losses, the losses in the stator magnetic circuit for hysteresis and eddy currents are also 28–30%; 20% account for aerodynamic losses and 10% for the losses in the permanent magnets and the rotor shroud, caused by eddy currents due to time and space harmonics. As can be seen, the main losses within the above power ranges and rotor rotational speeds are generated in the stator magnetic circuit and windings.

In our work, we resolve the issue of minimization of the losses in the HSEMPM magnetic stator circuit by using amorphous iron, and develop two HSEMPM projects: an electric power generator of 100 kW and a rotor speed of 60,000 rpm and an electric power generator of 200 kW with a rotor speed of 45,000 rpm for use in distributed power generation plants. The HSEMPM stator magnetic circuit in both projects is made of amorphous iron according to our proposed technology, which allows making electrical machines with a power of more than 100 kW. This result is new and is not presented in publications. One of the main requirements to the electric machines that we create is the minimum axial length. To fulfill this requirement, the electrical machines are made with tooth winding. But the number of slots per pole and phase is not fractional, which allows, in contrast to the known works on HSEMPMs with tooth winding, to minimize the spatial MMF harmonics and, accordingly, the eddy current losses in permanent magnets due to these harmonics. The article provides the results of calculations of two HSEMPMs using FEMM methods. The HSEMPM parameters obtained are compared with the HSEMPM prototype with a distributed winding and the magnetic circuit of electrical steel made by us earlier. Upon the results of these comparisons, we conclude on the appropriateness of the solutions proposed for HSEMPM. The rotor of HSEMPM studied is made from a single cylindrical SmCo magnet. According to the research, we have created a prototype of the stator magnetic circuit of amorphous iron and experimentally measured the losses in it.

2. HSEMPM WITH A MAGNETIC CIRCUIT OF AMORPHOUS IRON

Research on creation of electrical machines with magnetic circuits of amorphous iron is actively conducted by Hitachi for low-power electrical machines (up to 5 kW) [23, 24]. Publications do not provide information on electrical machines with a magnetic circuit of amorphous iron for higher power. This is due to several factors:

- The thickness of an amorphous iron strip does not exceed 25–30 microns. This virtually makes it possible to make magnetic circuits of amorphous steel mostly twisted. In some cases, it is possible to use laser cutting to make magnetic circuits, but the cost of the magnetic circuit manufacturing becomes significant.

- Amorphous iron has a low induction of saturation, which usually varies from 1.3 to 1.6 T. When doping amorphous iron with Co, magnetic induction increases to 1.8 T. But this also increases the specific losses due to the increase in electrical conductivity.

- The filling factor of the magnetic circuits of amorphous iron varies usually from 0.7 to 0.8. This is due to the fact that in production of amorphous iron, various technological sinks and blotches form on the strip.

All these features do not allow using HSEMPM with magnetic circuits of amorphous iron with known structural schemes. Therefore, in most cases, amorphous iron is used in non-slot HSEMPM designs [25, 26] or in axial electric machines.

To use amorphous iron in the HSEMPM stator of more than 100 kW, we offer the following approach: several triangular magnetic circuits are made of amorphous iron strip. The number of triangular magnetic circuits corresponds to the number of HSEMPM stator slots. It is important to note that to minimize economic costs in production, it is desirable that the number of these slots

was minimal. Triangular magnetic circuits are made by mounting the annular magnetic circuits of amorphous iron in the mandrel with slots of triangular shape and filling them with epoxy resin with special binders with subsequent heat treatment. In this mandrel, the annular magnetic circuits of amorphous iron take a triangular shape and obtain the required mechanical strength. Figure 1 shows our technological mandrel with triangular magnetic circuits in it. Figure 1 also shows our magnetic circuits of amorphous iron with a thickness of 25 microns after heat treatment. Next, one of the angles of triangular magnetic circuits is cut forming slotted part of HSEMPM, by mounting triangular magnetic circuits in the annular part, which simultaneously serves as a fastening element of the magnetic circuit and the stator back. After installation of triangular magnetic circuits, epoxy resin is filled again in the annular part followed by heat treatment.

The advantage of the proposed design scheme, in addition to the fact that it allows making the stator magnetic circuit with minimal specific losses, is that, because of its manufacturing technology, the technological channels for HSEMPM cooling (Figure 2) are formed, through which the coolant can pass. These channels are in the stator body, which significantly improves heat dissipation from the active HSEMPM zone. Therefore, in HSEMPM with magnetic circuit of amorphous iron, we use air

(a) (b)

Figure 1. Technological mandrel with magnetic circuits of (a) amorphous iron and (b) triangular magnetic circuits.

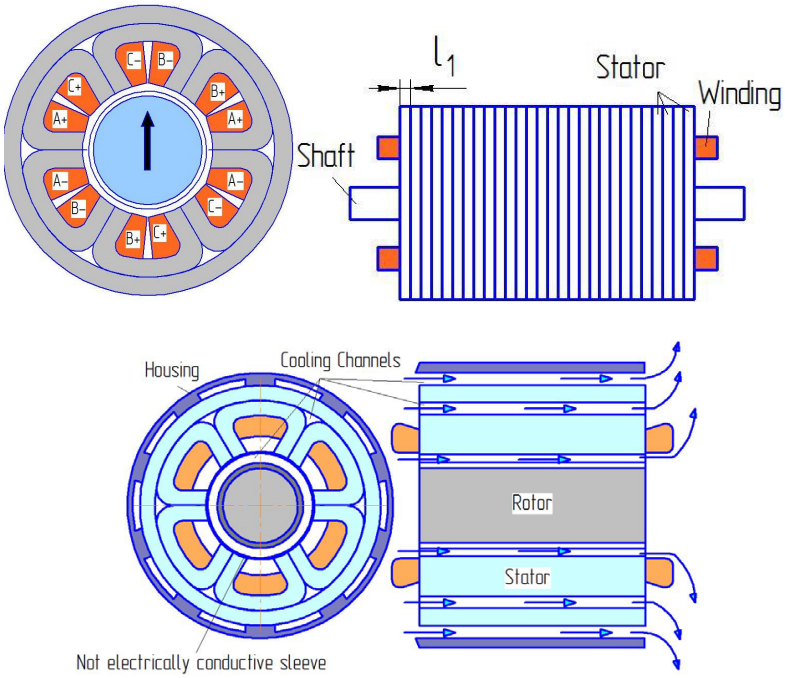

Figure 2. HSEMPM with a magnetic circuit of amorphous iron and its cooling system.

as the cooling medium, which passes in three ways: in the stator body, in the air gap and in the stator surface. We installed a ceramic sleeve in the gap between the stator and the rotor to minimize aerodynamic losses.

Figure 2 shows HSEMPM made according to our technology. To minimize losses due to eddy currents and hysteresis, the stator is assembled of multiple magnetic circuits, the axial length ($l1$) is 3 to 5 mm each. It is also possible to achieve a smaller axial length, but at the same time the circuit assembly technology becomes more complicated, and its cost increases.

When manufacturing a magnetic circuit using this technology, the waste material is no more than 10–12%; in the traditional manufacturing of magnetic circuits the waste material exceeds 30%. Making two such magnetic circuits for electrical machines of 100 kW at the mass-production metallurgical plant, taking into account the cost of material, technological development and manufacturing cost us $1,000. For comparison, making one magnetic circuit of electrical steel for the electric machine of similar power is $1,200 to $2,000, depending on the manufacturing technology.

3. DESIGN

To evaluate the effectiveness of the proposed solution, we performed calculations of two HSEMPMs with magnetic circuits implemented according to the proposed technology. The results of calculations of these HSEMPMs were compared with the parameters of HSEMPM prototype with the distributed winding and the magnetic circuit of electrical steel, made by us earlier [27]. The calculation schemes of the designs are given in Figure 3.

The rotor of HSEMPM designed was made of 6 of cylindrical SmCo magnets ($B_r = 1,07$ T; $H_c = 756$ kA/m) with a diameter of 60 mm and an axial length of 25 mm. The rotor is made with the layer magnets to reduce the eddy current losses in permanent magnets due to spatial and time harmonics. The stator is made of amorphous iron of 5CP grade (manufactured by Ashinsky Steel Works) with a saturation induction of 1.35 T and specific losses at a frequency of 1,000 Hz and induction of 1.25 T not more than 5 W/kg. These values are obtained considering the fact that the core is assembled from magnetic circuits with an axial length of 5 mm.

As noted above, in order to reduce economic costs in the production of HSEMPM with a magnetic circuit of amorphous iron, the minimum number of slots shall be chosen. Therefore we made HSEMPM with 6 slots, and 2 poles. The HSEMPM winding is a tooth winding, made with multiple core wire, a total cross section of 54 mm^2 and a core diameter of 0.8 mm. Wire insulation was of polyimide, a temperature index of 220°C. The number of slots per pole and phase in this case was 1, i.e., an integer, rather than a fraction, which is typical for electrical machines with tooth winding. The integer number

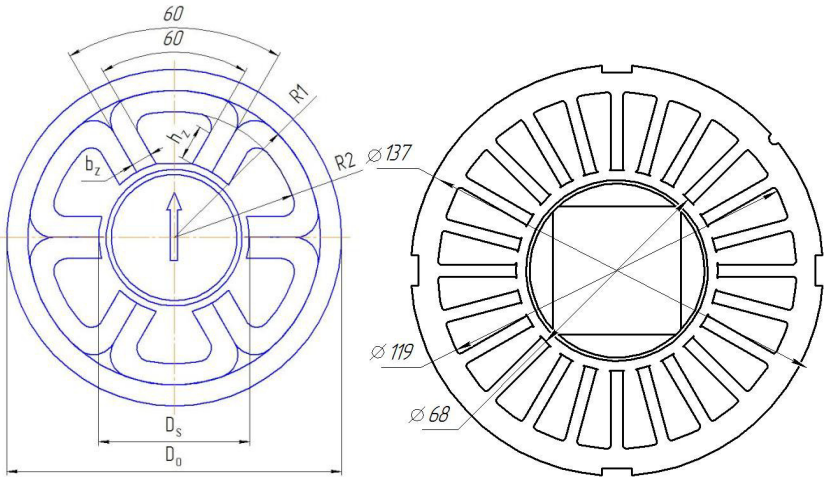

(a) (b)

Figure 3. HSEMPM studied: (a) with a magnetic circuit of amorphous iron and tooth winding; (b) with distributed winding and the stator magnetic circuit of electrical steel.

of slots per pole and phase in our case allows minimizing spatial MMF harmonics and the losses for the eddy currents generated by them in the magnets and the rotor shroud.

When selecting the size of HSEMPM designed, dimensions of the stator magnetic circuit were chosen in order for induction in the teeth and the back to be the same. In this case, the specific losses in the teeth and the back will be the same, and the total losses in the stator iron will depend on the weight of the back and the teeth. In HSEMPM a distributed winding and the magnetic circuit of electrical steel, it is difficult to achieve the same weight of the teeth and the back, so distribution of losses in the stator magnetic circuit is almost always uneven therein. For two-pole HSEMPM with a drop-forged magnetic circuit, losses in the HSEMPM stator back are greater than losses in the teeth.

In HSEMPM made according to our proposed technology, the stator back is formed separately from the teeth, achieving approximately the same weight of the back and the teeth (the difference between the weights is not more than 20–30%). Then distribution of losses in the stator iron is almost even. It should be noted that the stator back (an annular magnetic circuit where triangular magnetic circuits of amorphous iron are inserted) can be made, for example, from cobalt alloys with high saturation induction. This will minimize the weight of the back and, when choosing certain ratios, achieve optimal losses in the HSEMPM stator magnetic circuit. We do not consider such magnetic circuits in this paper; they will be studied by us in subsequent works.

Initially, HSEMPM calculations were performed using the analytical methods given in [27, 28]. Clarifying calculations were performed using Ansys Maxwell software package.

In calculations, two different HSEMPM sizes were considered for different power, rotor speed and the output voltage: 120 kW at a speed of 60,000 rpm and phase voltage of 115 V, and 200 kW at a speed of 45,000 rpm and phase voltage of 220 V. Rotor speeds, voltage and power of electrical machines were specified in the terms of reference.

HSEMPM calculations were performed for four modes of operation: idling, three-phase short circuit, work under load with $\cos\varphi = 1$ and $\cos\varphi = 0.8$. The geometrical dimensions and design parameters of HSEMPM are given in Table 1.

Table 1 shows that because of the low saturation induction of amorphous iron, weight in options A and B is greater than that of option C (with distributed windings and the magnetic circuit of electrical steel). At the same time, due to the use of tooth winding, the overall length of HSEMPM being developed is 50 mm less than the analog with distributed winding. The cost of HSEMPM with tooth winding and magnetic circuit made according to our technology is less than HSEMPM with distributed winding. In general, it can be concluded from the above calculations on the effectiveness of our HSEMPM with magnetic circuit of amorphous iron and tooth winding. Also, our technology of making a magnetic circuit allows to achieve more intensive cooling HSEMPM due to channels in the stator body. Therefore, unlike HSEMPM with distributed winding, we use air as a coolant; its flows are formed by the impeller installed on the rotor.

Next, for complete assessment of the effectiveness of the above HSEMPM, the results of its calculations with FEMM methods are given. Figure 4 shows the results of computer simulation of the magnetic field and losses in the permanent magnet of HSEMPM rotor with tooth winding and a power of 120 kW and the rotor speed of about 60000 rpm for different modes of HSEMPM operation. Table 2 shows the harmonic spectrum of voltages and currents for $\cos\varphi = 1$ and $\cos\varphi = 0.8$. Figure 5 shows the electromagnetic torque in HSEMPM at three-phase short circuit.

As can be seen in Figure 4, the maximum value of the magnetic induction in the teeth of HSEMPM does not exceed 1.25 T, and induction in the teeth of the stator and the stator back is evenly distributed. Also, in Figure 4 it can be seen that at $\cos\varphi = 0.8$ losses in permanent magnets due to eddy currents caused by spatial harmonics increase by 10%. It should be noted that at a three-phase short circuit, losses in the permanent magnets of the rotor increase by almost 8–10 times. This can lead to demagnetization of permanent magnets from overheating. This result should be taken into account when designing HSEMPM with tooth winding. In general, the results of computer simulation, and distribution of magnetic fields and losses prove working efficiency of our constructive scheme and its possible practical implementation. Also, the FEMM results prove correctness of dimensions obtained in Table 1.

By analyzing the harmonic structure of currents and voltages, it can be seen that in load modes of HSEMPM, 3rd and 5th harmonics of current voltage are not more than 3% of the rated. This is

Table 1. HSEMPM parameters.

Option	A	B	C
Power, kW	200	120	120
The number of the rotor poles	2	2	4
The number of stator slots	6	6	24
Rotor speed, rpm	45000	60000	60000
No-load voltage, phase, active, V	231	125	125
Voltage at rated load, $\cos\varphi = 1$ (load), phase, active, V	217	121	117
Voltage at rated load, $\cos\varphi = 0,8$ (load), phase, active, V	212	115,71	110
Rated current, $\cos\varphi = 1$ (load) phase, active, A	301	342	345
Rated current, $\cos\varphi = 0.8$ (load) phase, active, A	357	422	427
Current density A/mm^2	6	6	8
Linear current load, A/m	111836	72600	77557
Short-circuit current, A	1580	1600	1100
The number of turns per phase	14	8	8
Magnetic induction in the stator back, T	1.25	1.25	1,4
Magnetic induction in the stator teeth, T	1.25	1.25	1,4
Magnetic induction in the air gap, T	0.6	0.6	0,65
Active stator length, mm	210	150	165
D_s, mm	72	72	68
D_o, mm	190	160	137
$R1$, mm	80	60	–
$R2$, mm	90	70	–
b_z, mm	20	20	–
h_z, mm	35	19	–
Material	Thickness of 25 microns	Thickness of 25 microns	Silicon steel 0.18 mm
Induction of saturation, T	1,35	1,35	1,8
The cost of magnetic circuit manufacturing, $	700	500	1200
Rotor diameter, mm	60	60	60
Type of permanent magnets, B_r(ТП)/H_c(κА/М)	SmCo, 1.07/756	SmCo, 1.07/756	SmCo, 1.07/756
Shroud thickness, mm	4	4	4
Shroud material	Carbon	Carbon	Carbon
Limit of strength of the shroud material, MPa	1880	1880	1880
Mass of active parts, kg	28	21	19
Stator length with frontal parts, mm	210	190	240
Coolant	Air	Air	Water

achieved by the fact that we use tooth winding with a integer number of slots per pole and phase in our project. That is why losses in permanent magnets caused by spatial MMF harmonics in our project are significantly less than in common electrical machines with tooth winding and a fractional number of slots per pole and phase. Also as a result of computer simulation, it can be seen that even harmonics appear in short circuit. For our dimensions and numerical parameters, voltage at the three-phase short-circuit at the HSEMPM terminals had 8th harmonic, the amplitude of which is not more than 5% of the rated voltage.

However, it is evident that a significant increase in the eddy current losses in the permanent magnets is not caused by harmonic current spectrum, but substantial increase of a current (current increases more than 5 times).

An important task that requires special attention when designing HSEMPM is to analyze the processes in HSEMPM at short circuit, since it is the most negative operating mode for electric machines with permanent magnets. Therefore, in computer simulation, we also considered the processes

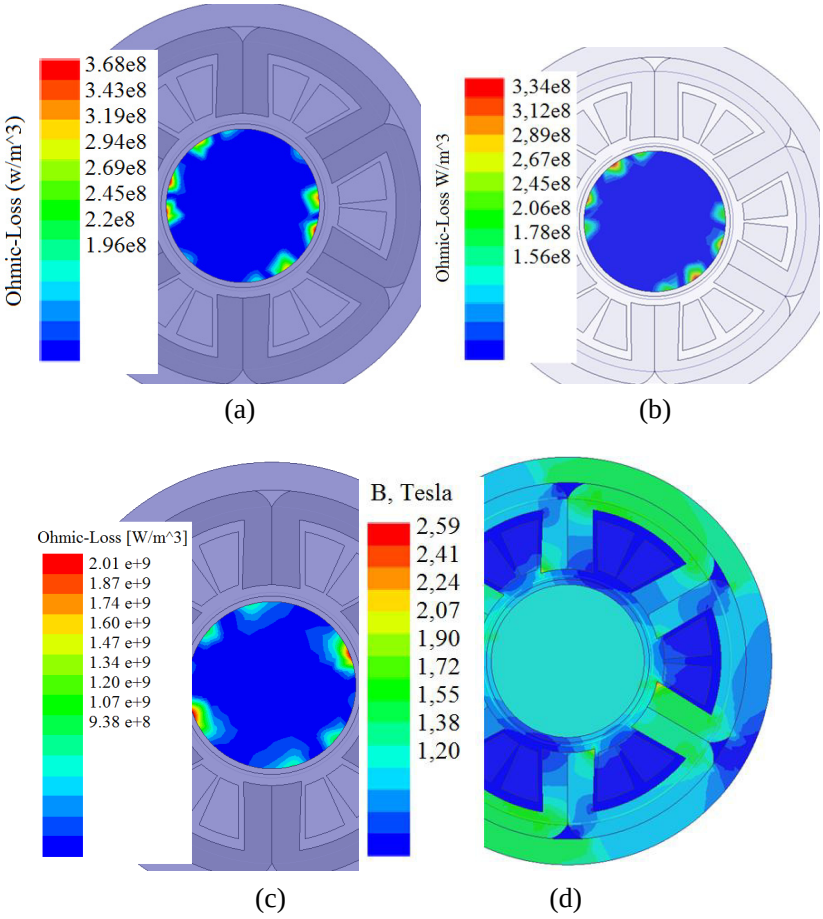

Figure 4. Computer simulation results: (a) Eddy current losses in HSEMPM with tooth winding, a power of 100 kW at $\cos\varphi = 0.8$, at a speed of 60,000 rpm under rated load; (b) Eddy current losses in HSEMPM with tooth winding and a power of 100 kW at $\cos\varphi = 1$; (c) Eddy current losses in HSEMPM with tooth winding and a power of 100 kW at short circuit; (d) Distribution of the magnetic field in the HSEMPM stator magnetic circuit.

Table 2. Harmonic spectrum of currents and voltages for different modes of HSEMPM operation.

	U_1, V	I_1, A	U_3, V	I_3, A	U_5, V	I_5, A	U_7, V	U_8, V
$\cos\varphi = 1$	160	–	5	–	–	–	–	–
$\cos\varphi = 0.8$	139.08	488	4.7	15.16	–	13.52	–	–
Short circuit	12.1	–	0.32	–	–	–	0.3	0.45

in HSEMPM at sudden three-phase short circuit.

Figure 5 shows an electromagnetic torque in HSEMPM (topology B) at sudden three-phase short circuit (the initial speed is 60,000 rpm), and Figure 6 shows the magnetic field distribution in the permanent magnet with a three-phase short circuit. The speed is consistent with the electric period.

The analysis of Figure 5 shows that in three-phase short circuit, the peak value of the electromagnetic torque in HSEMPM at the first milliseconds of the transient process reaches 125 Nm. This value is more than 6 times the nominal electromagnetic torque and may lead to disturbance of mechanical connection between the turbine and HSEMPM. This large value of the electromagnetic torque at the short circuit is caused by a significant air gap in HSEMPM. It is therefore evident that the short-circuit currents in HSEMPM shall be limited (for example, this can be achieved by adding an

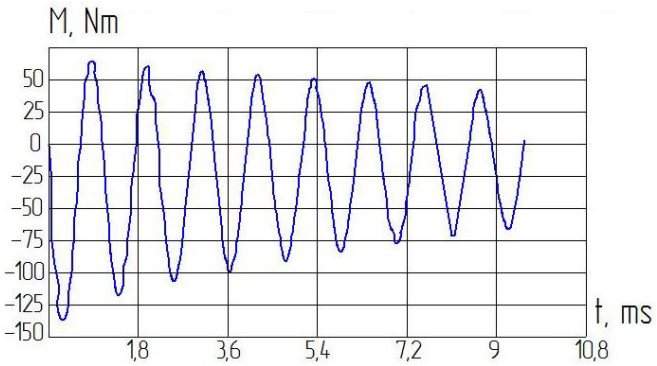

Figure 5. Electromagnetic torque at sudden three-phase short circuit.

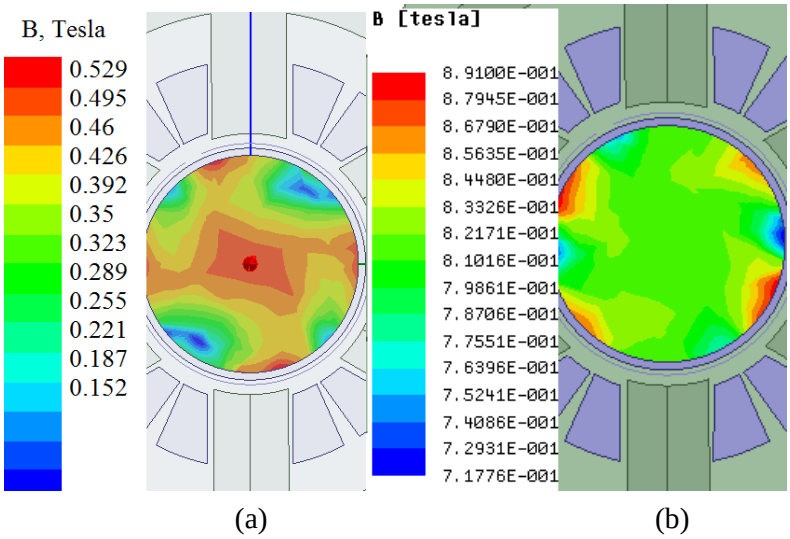

Figure 6. Magnetic field distribution in the permanent magnet at (a) short circuit and (b) idling.

additional inductance [2, 3]).

As seen in Figure 6, the permanent magnet at the sudden three-phase short circuit is not demagnetized by the effect of short-circuit currents. Magnetic induction therein decreases by 2 times. In this case, it should be noted that although the magnet is not demagnetized by the effect of short-circuit currents, taking into account the increase in losses due to eddy currents in it by 10 times, the magnet may still demagnetize, but caused by the combined effect of heat and electromagnetic fields.

We obtained similar results for 200 kW HSEMPM and a rotor speed of 45,000 rpm. Since the phase voltage of 200 kW HSEMPM (topology A) was almost 2 times higher, this HSEMPM (topology B) was made based on the above-described 120 kW HSEMPM with linear increase in the current load (the number of turns in the winding), and respectively, overall stator dimensions. That is, the topology A was obtained from the topology B by increasing the active length and decreasing the number of turns. The HSEMPM rotor remained unchanged in terms of the outer diameter; only the active length was changed. This decision was made for a subsequent HSEMPM unification in mass production. Dimensions of 200 kW HSEMPM are shown in Table 1. Figure 7 shows the results of computer simulation of the magnetic field distribution and the loss in the rotor of 200 kW HSEMPM with a rotor speed of 45,000 rpm.

The analysis of computer simulation results shows that the value of magnetic induction in the stator magnetic circuit is 1.25 T, the magnetic induction in the stator teeth and stator back is the same achieving a uniform distribution of the losses in the stator magnetic circuit. The eddy current losses in the permanent magnets of the rotor of 200 kW HSEMPM due to time harmonics are 30% less, compared to 100 kW HSEMPM. This is because the current frequency in 200 kW HSEMPM is 30% less than in

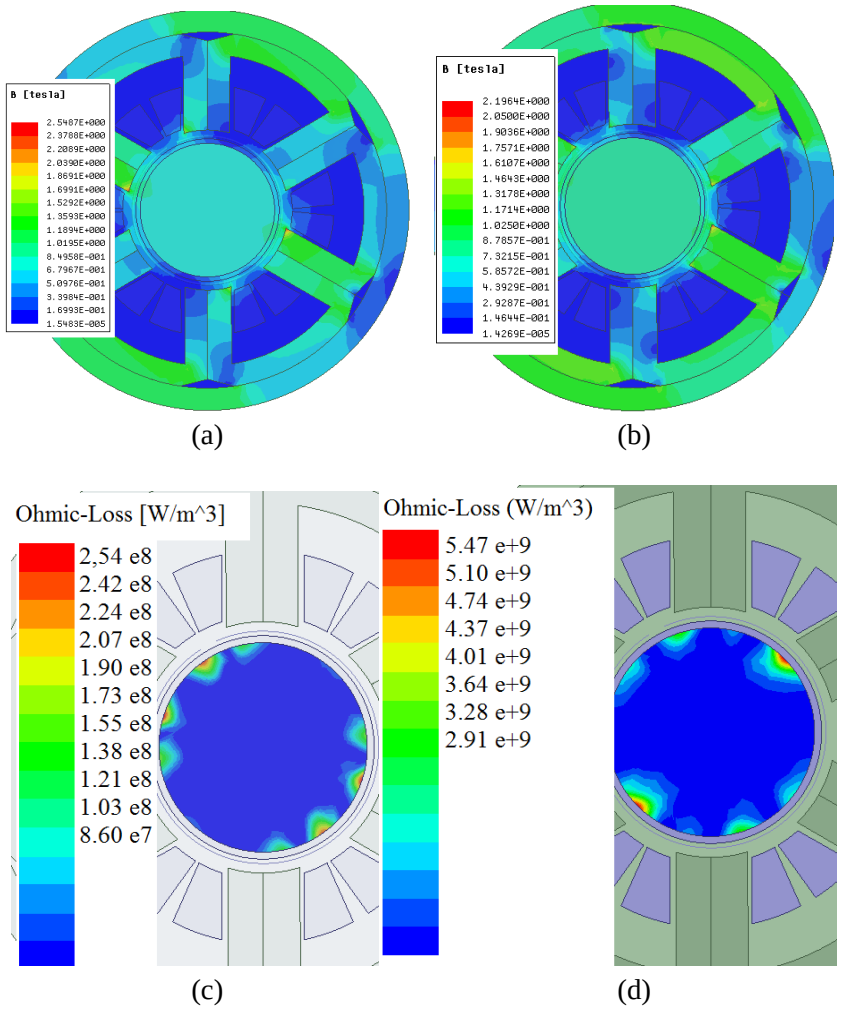

Figure 7. Computer simulation results: (a) Magnetic field distribution in the stator magnetic circuit of 200 kW HSEMPM at no-load; (b) Magnetic field distribution in the stator magnetic circuit of 200 kW HSEMPM at nominal load; (c) Eddy current losses in HSEMPM with tooth winding and a power of 200 kW at $\cos\varphi = 1$; (d) Eddy current losses in HSEMPM with tooth winding and a power of 200 kW at short circuit.

100 kW HSEMPM. Of course the eddy current losses are not linearly dependent on the frequency. In our case, a linear relationship was obtained by accident due to a simultaneous change in the number of turns, the frequency of current in HSEMPM windings and overall stator dimensions.

In general, in terms of thermal load, 200 kW HSEMPM is similar to 100 kW HSEMPM. This is due to the increase in the phase and output voltage of 200 kW HSEMPM. To maintain a low current density, 200 kW HSEMPM slot dimensions were 2–2.5 times increased compared to 100 kW HSEMPM.

Thus, the results of FEMM confirm working efficiency of our technology. The next stage of our research was to evaluate the effectiveness of the proposed technical solution and its comparison with HSEMPM with distributed winding and electrical steel magnetic circuit.

4. EVALUATING THE EFFECTIVENESS OF OUR HSEMPM AND EXPERIMENTAL STUDIES OF LOSSES

Since the primary goal is to minimize losses in HSEMPM, losses in parts of HSEMPM were initially studied for evaluating the effectiveness of the use of our technology. The results of these calculations are given in Table 3.

Stator winding losses were calculated by known methods, and for HSEMPM with distributed

Table 3. Losses HSEMPM obtained by calculation.

HSEMPM	A	B	C
Aerodynamic losses, W	463	800	874
Losses in the stator winding, W	2385,9	1498	1274
Losses in the stator magnetic circuit, W	340	254	1238
Eddy current losses in the permanent magnets, W	276	348	227
Total losses, W	3464.9	2900	3613
Efficiency, %	98	97.6	97

winding and magnetic circuit of electrical steel, they have been measured experimentally in the prototype developed by us earlier. The results of evaluation of the eddy current losses in the permanent magnets, rotor shroud and rotor iron due to spatial harmonics are considered above by FEMM methods. Losses due to time harmonics were calculated based on the results of [29] and are given in Table 3. The aerodynamic losses and losses in the stator magnetic circuit were studied experimentally. The need for these studies was caused by the fact that the stator formation technology proposed by us is new and not considered in the literature, and there is also no method for determining the losses for hysteresis losses and eddy currents.

Determining aerodynamic losses. To evaluate the aerodynamic losses and to determine the HSEMPM rotor diameter, it is expedient to use equations from [30]:

$$P_{\text{air}} = \frac{c_f \pi \rho_{\text{BO3}} \Omega^3 D_b^4 l}{16} \tag{1}$$

where c_f — coefficient of friction between rotors and environment; ρ_{BO3} — air density; D_b — rotor diameter; Ω — rotor speed, rad/s; l — length of section where losses are determined.

The main difficulty when using this expression is the difficulty of determining the coefficient of rotor-air friction. Usually, solving this problem requires calculating the Reynolds number for the air environment, which will depend on purity of the rotor surface treatment, air gap and other parameters that are difficult to calculate with reasonable accuracy. Another method of determining the losses is to provide a three-dimensional model and analyze it by FEMM methods. Solution of hydrogasdynamics tasks using FEMM is a very time-consuming process unlike the electromagnetic calculations.

Therefore, in our work, friction coefficient for our rotor was determined experimentally. Figure 8 shows a setup for measuring the aerodynamic losses of the rotor. Using this setup, the rotor was accelerated to 21,000 rpm and its temperature was measured. We measured energy losses at this temperature, and then, based on the dimensions and the rotor speed determined the coefficient of air-rotor friction using expression (1).

As a result of our experimental studies, it was established that friction coefficient is 0.007 for our rotor. At a speed of 21,000 rpm, the test rotor temperature was 44°C, which corresponds to 34 W. Then, based on the value of the rotor-air friction coefficient obtained experimentally (that does not change

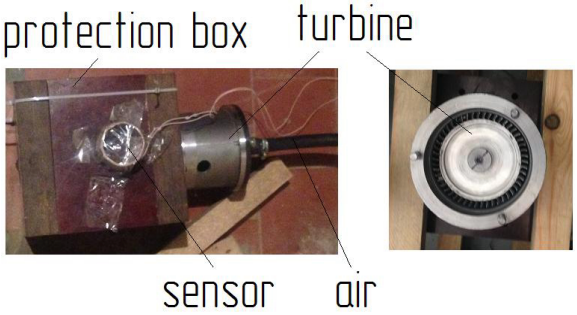

Figure 8. A setup for technological rotor spin.

when the geometry and the sizes change), we determined the aerodynamic losses for all HSEMPM options with respect to their geometric dimensions.

Determining losses in the stator iron for magnetic polarity reversal and eddy currents. Since our topology is new, the use of known methods for calculation of losses in the stator magnetic circuit in this case can lead to a rather large error. Therefore, to evaluate losses in the HSEMPM stator magnetic circuit, we studied losses in the stator core at high frequency of magnetic polarity reversal at magnetometer. The principle of operation of magnetometer is reversal of the ring sample of a soft magnetic material with two windings: measuring and power. Reversal is carried out on a dynamic hysteresis loop at frequencies of 50–3,000 Hz, the voltage across the power winding is assumed to be specified. As a result of the measurements, magnetic hysteresis loops are recorded, and specific losses are determined by wattmeter method.

In Figure 9, voltmeter PV1 measures half-period average voltage and subsequently determines the amplitude of magnetic induction, and voltmeter RV2 measures the effective value of voltage and subsequently determines its curve shape factor. These voltmeters measure within a range of 30 mV to 100 V, the maximum input current is not more than 5 mA. Wattmeter PW measures active power and subsequently determines the specific magnetic losses. It has a measurement range of 0.75 to 30 Watts. Ammeter RA measures the effective value of the magnetizing current and subsequently determines the effective value of the magnetic field and has a measuring range of 0.1 to 5.0 A. Frequency meter PF measures the frequency with accuracy within ±0.2%. G — power supply.

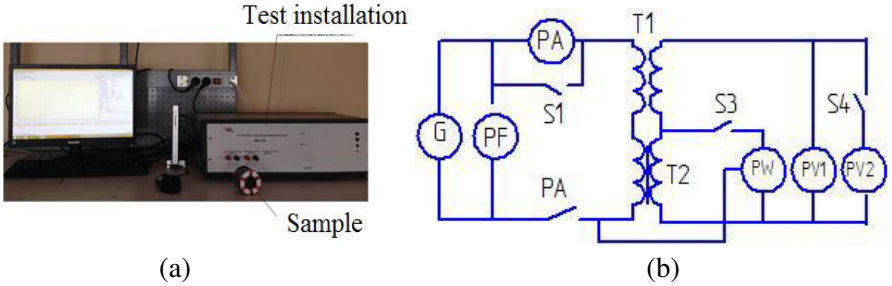

Figure 9. Setup to study losses in (a) magnetic circuit and (b) the setup diagram.

Determining the specific magnetic losses by this method is based on measuring the active power consumed for magnetic polarity reversal and power consumed by measuring devices (wattmeters and voltmeters) and the amplifier feedback circuit. Active power is determined indirectly by the voltage on the test sample winding. Determining the effective value of the magnetic field strength is based on the measurement of magnetizing current.

Accuracy of measurement by this method was not more than 2.5%. As a result of measuring losses of complete magnetic circuits, we have found that losses in the magnetic circuit created by us at magnetic polarity reversal frequency of 1,000 Hz and induction of 1.25 T are not more than 5 W/kg. At a frequency of 3,000 Hz, specific losses were 19 W/kg, which is also a very good result.

Evaluating the effectiveness of the proposed topology. Losses HSEMPM obtained by calculation are given in a Table 3.

When comparing two HSEMPMs of equal power at the same rotor speed (100 kW, 60,000 rpm), it can be seen that losses in the proposed design scheme are 700 watts less. Moreover, this advantage is achieved only by reducing the losses in the stator magnetic circuit for eddy currents and hysteresis. Winding losses and losses in the permanent magnets for eddy currents in the proposed HSEMPM are higher than in HSEMPM with distributed winding and magnetic circuit of electrical steel. Reducing losses by 700 watts at increasing cooling intensity, by introducing additional channels in the stator body can significantly reduce heating of the HSEMPM active elements, which of course is a significant advantage.

It should be noted that the proposed constructive scheme has an overall length less than 50 mm than its analog, wherein the weight of the proposed HSEMPM is 1 kg more than that of the analog. But the cost of manufacturing of our constructive scheme, taking into account a minimum of wastes, is almost 2 times less than that of the analog.

It is obvious that all these advantages show a higher efficiency of the proposed structural scheme and allow recommending it to practical use.

According to the projects developed, in the future, we will create two full-size prototypes and conduct their full-scale testing.

5. RESULTS AND CONCLUSIONS

Thus, we have proposed a technology and constructive HSEMPM with magnetic circuit of amorphous iron. Its effectiveness and appropriateness of application is proven. Two HSEMPM projects were developed: a 100 kW power generator with a rotor speed of 60,000 rpm and a 200 kW power generator with a rotor speed of 45,000 rpm for use in the distributed power generation plants. The HSEMPM stator magnetic circuit is made of amorphous iron in both projects according to our technology, which allows making electrical machines with a power of more than 100 kW. According to the studies, we have created a prototype of the stator magnetic circuit of amorphous iron and experimentally measured losses in it, as well as provided results of experimental research of aerodynamic losses.

ACKNOWLEDGMENT

The work was supported by the Russian Science Foundation, project 17-79-20027.

REFERENCES

1. Uzhegov, N., J. Pyrhonen, and S. Shirinskii, "Loss minimization in high-speed permanent magnet synchronous machines with tooth-coil windings," *IECON 2013 — 39th Annual Conference of the IEEE Industrial Electronics Society*, 2960–2965, 2013.
2. Ganev, E., "High-performance electric drives for aerospace more electric architectures," *IEEE Power Engineering Society Meeting*, 1–8, 2007.
3. Ganev, E., "Selecting the best electric machines for electrical power generation systems," *IEEE Electrification Magazine*, Dec. 2014.
4. Besnard, J.-P., F. Biais, and M. Martinez, "Electrical rotating machines and power electronics for new aircraft equipment systems," *ICAS-Secretariat — 25th Congress of the International Council of the Aeronautical Sciences*, 2006.
5. Nagorny, A., N. Dravid, R. Jansen, and B. Kenny, "Design aspects of a high speed permanent magnet synchronous motor/generator for flywheel applications," NASA/TM-2005-213651, 1–7, 2005.
6. Bobtsov, A. A., A. A. Pyrkin, R. Ortega, et al., "A robust globally convergent position observer for the permanent magnet synchronous motor," *Automatica*, Vol. 61, 47–54, 2015.
7. Zhu, Z. Q., "David howe electrical machines and drives for electric, hybrid, and fuel cell vehicles," *Proceedings of the IEEE*, Vol. 95, No. 4, 746–765, 2007, DOI: 10.1109/JPROC.2006.892482.
8. Chin, Y. K., "A permanent magnet synchronous motor for traction application of electric vehicle," *IEEE Int. Electric Machines and Drive Conference*, Vol. 2, 1035–1041, 2003.
9. Gieras, J. F., "High speed machines," *Advancements in Electric Machines (Power Systems)*, 81–113, 2008.
10. Bailey, C., D. Saban, and P. Guedes-Pinto, "Design of high-speed direct-connected permanent-magnet motors and generators for the petrochemical industry," *IEEE Transactions on Industry Applications*, Vol. 45, No. 3, 1159–1165, 2009.
11. Carlson, R. and F. Wurtz, "Optimal design of a set of permanent magnet generators with the same cross-section," *J. Microw. Optoelectron. Electromagn. Appl.*, Vol. 12 No. 2, 678–693, São Caetano do Sul, Dec. 2013.
12. Abdi, B., J. Milimonfared, and J. Moghani, "Simplified design and optimization of slotless synchronous PM machine for micro-satellite electro-mechanical batteries," *Advances in Electrical and Computer Engineering*, Vol. 9, No. 3, 84–88, 2009.

13. Borisavljevic, A., H. Polinder, and J. Ferreira, "On the speed limits of permanent-magnet machines," *IEEE Transactions on Industrial Electronics*, Vol. 57, No. 1, 220–227, 2010.
14. Munteanu, G., A. Binder, and T. Schneider, "Loss measurement of a 40 kW high-speed bearingless PM synchronous motor," *IEEE Energy Conversion Congress and Exposition: Energy Conversion Innovation for a Clean Energy Future, ECCE 2011, Proceedings2011*, Article number 6063841, 722-729, 2011.
15. Johnson, D., P. Pillay, and M. Malengret, "High speed PM motor with hybrid magnetic bearing for kinetic energy storage," *Conference Record — IAS Annual Meeting (IEEE Industry Applications Society)*, Vol. 1, 57–63, 2001.
16. Ismagilov, F., I. Khairullin, V. Vavilov, and M. Gumerova, "Application of hybrid magnetic bearings in aviation starter-generators," *International Review of Electrical Engineering*, Vol. 9, No. 3, 506–510, 2014.
17. Tuysuz, A., M. Steichen, C. Zwyssig, and J. W. Kolar, "Advanced cooling concepts for ultra-high-speed machines," *9th International Conference on Power Electronics — ECCE Asia: "Green World with Power Electronics", ICPE 2015-ECCE Asia*, 2194–2202, 2015.
18. Dajaku, G. and D. Gerling, "Magnetic radial force density of the PM machine with 12-teeth/10-poles winding topology," *IEEE International Electric Machines and Drives Conference, IEMDC 2009*, 157–164, Florida, USA, May 3–6, 2009.
19. Isomura, K., M. Murayama, S. Teramoto, K. Hikichi, and Y. Endo, "Experimental verification of the feasibility of a 100 W class micro-scale gas turbine at an impeller diameter of 10 mm," *J. Micromech. Microeng.*, Vol. 16, 254–261, 2006.
20. Vavilov, V., F. R. Ismagilov, I. Hairullin, and D. Gusakov, "High efficiency ultra-high speed microgenerator," *Conf. Rec. IEEE IECON*, 2016.
21. Gerling, D. and M. Alnajjar, "Six-phase electrically excited synchronous generator for more electric aircraft," *International Symposium on Power Electronics, Electrical Drives, Automation and Motion*, 7–13, 2016.
22. Huynh, C., L. Zheng, and D. Acharya, "Losses in high speed permanent magnet machines used in microturbine applications," *Journal of Engineering for Gas Turbines and Power*, Vol. 131, No. 2, 1–6, 2009.
23. Wang, Z., et al., "Development of a permanent magnet motor utilizing amorphous wound cores," *IEEE Transactions on Magnetics*, Vol. 46, No. 2, 570–573, Feb. 2010.
24. Wang, Z., et al., "Development of an axial gap motor with amorphous metal cores," *IEEE Trans. Ind. Appl.*, Vol. 47, No. 3, 1293–1299, May/Jun. 2011.
25. Pabut, O., M. Kirs, H. Lend, and T.Tiirats, "Optimal structural design of a slotless permanent magnet generator," *Proceedings of the International Conference of DAAAM Baltic "Industrial Engineering"*, Vol. 2015, 75–81, Jan. 2015.
26. Koo, M., J.-Y. Choi, J.-H. Jeong, H.-J. Shin, and K. Hong, "Characteristic analysis of permanent-magnet synchronous generator with slotless stator structure considering magnetic/mechanical air gap using semi-3-D analytical method," *IEEE Transactions on Magnetics*, Vol. 51, No. 11, 87–92, Nov. 1, 2015.
27. Yakupov, A., F. Ismagilov, I. Khayrullin, and V. Vavilov, "Method of designing high-speed generators for the biogas plant," *International Journal of Renewable Energy Research*, Vol. 6, No. 2, 447–454, 2016.
28. Uzhegov, N., E. Kurvinen, J. Nerg, J. T. Sopanen, and S. Shirinskii, "Multidisciplinary design process of a 6-slot 2-pole high-speed permanent-magnet synchronous machine," *IEEE Transactions on Industrial Electronics*, Vol. 63, No. 2, 784–795, Feb. 2016.
29. Zwyssig, C., J. W. Kolar, and S. D. Round, "Mega-speed drive systems: Pushing beyond 1 million RPM," *IEEE/ASME Transactions on Mechatronics*, Vol. 14, No. 5, 564–574, 2009.
30. Polinder, H. and M. J. Hoeijmakers, "Eddy-current losses in the permanent magnets of a PM machine," *EMD 97*, No. 444, Sep. 1–3, 1997.